Filament statistics with visible imaging and Langmuir probes

T. Farley*[1,2], F. Militello[2], N. Walkden[2], L. Kogan, J. Harrison[2], S. Silburn[2], J.W. Bradley[1]

[1]Department of Electrical Engineering and Electronics, Brownlow Hill, Liverpool, L69 3GJ, UK
[2]Culham Centre for Fusion Energy, Abingdon, Oxfordshire, OX14 3DB, UK

*tom.farley@ukaea.uk

Motivation

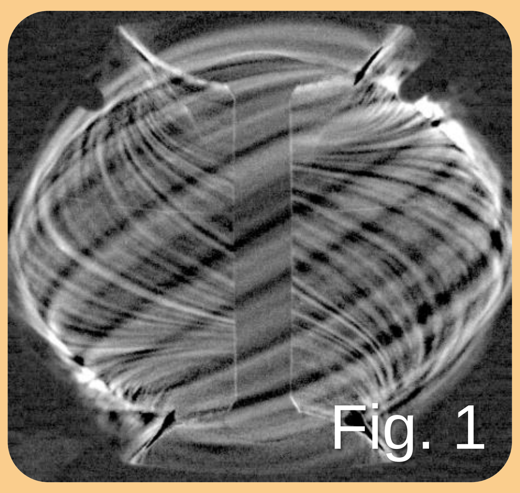
Fig. 1

- Coherent **filamentary structures** dominate tokamak turbulent cross-field particle transport [1]
- These intermittent structures' properties govern scrape off layer (SOL) **density profile shape** [2]
- Unfiltered **fast visible cameras** (~100 kHz) can passively collect large quantities of filament data
- A better understanding of filaments' dependence on plasma properties can help **minimise wall erosion** and **maximise machine lifetime**

Technique

- Unfiltered **fast camera** collects mostly D_α light
  - Intensity, I, function of neutral & electron density, n_0 & n_e, and electron temperature, T_e:
    - $I = n_0 f(n_e, T_e)$

1. Images processed to **enhance filaments**:
   - Background subtraction, noise reduction, sharpening
   - Image flattened to give image vector u_j
2. **Invert images**:
   - Trace field line (FL) grid with Efit++ equilibria
     - FLs parameterised by $(R, \phi R)$ coordinate of intersection with midplane ($Z = 0$)
   - Project FLs onto camera view
   - Stack flattened images of field lines to form **geometry matrix** G_i^j
   - The emission along field lines, P_i, is approximated by the "pseudo-inversion":

     $$P_i = G_i^j \, u_j$$
3. Full inversion is approximately recovered by regularised SART **point spread function** matrix inversion:
   - $\epsilon_k = P_i \left(G_j^i G_k^j\right)^{-1}$
   - Where $\left(G_j^i G_k^j\right)^{-1} = F_k^i$ is a point spread function matrix

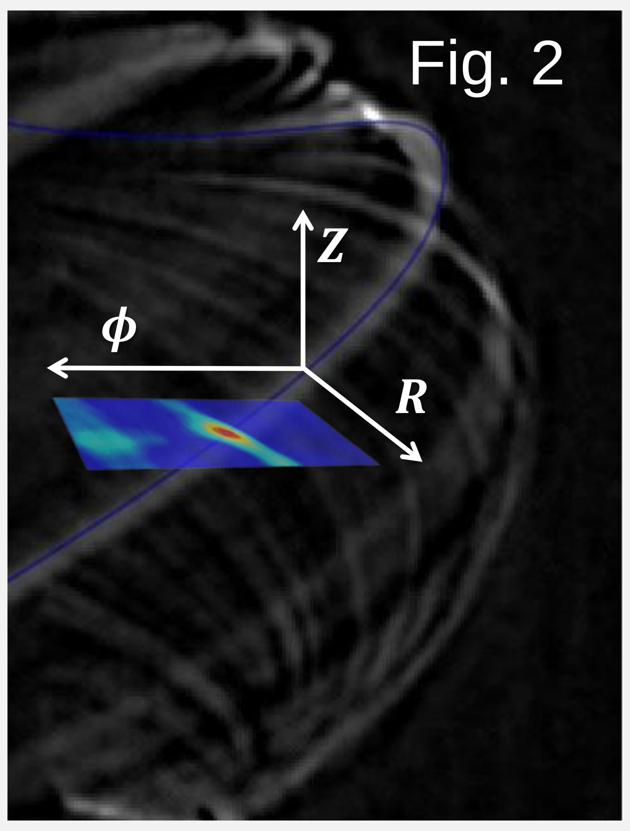

Fig. 2

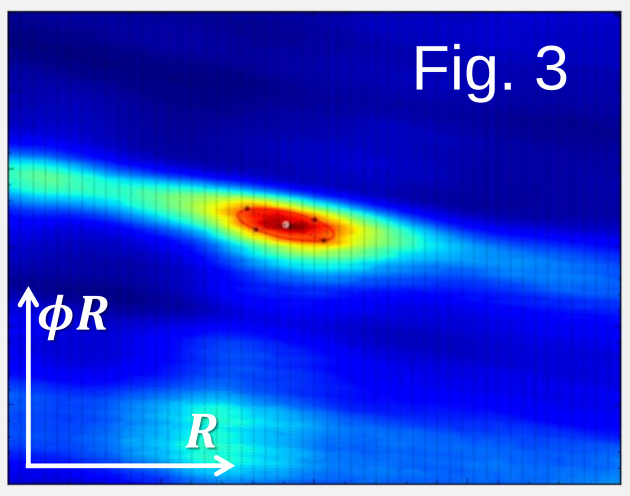

Fig. 3

Pseudo-Langmuir probe analysis

- Bulk of filament measurements in the literature have used Langmuir probe measurements
- Therefore important to compare new **fast camera** technique with **reciprocating Langmuir probe (RCP)** data for common refence point
- Slices through stacks of inverted frame data yield **1D data series** which can be treated with Langmuir probe statistical analysis techniques
  - **Temporal slices** give variation in average intensity along a given field line, similar to **RCP I_{sat} profiles**
  - **Radial slices** provide similar signals to reciprocating Langmuir probe radial profiles
  - **Peak detection** enables conditional averaging, waiting time, amplitude distribution measurements etc.

Fig. 4

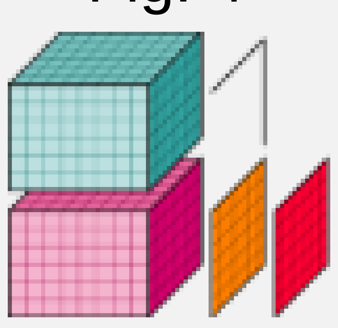
Credit: xarray project

Pulse information

- Ohmic, L-mode, connected double null (CDN) MAST plasmas

Parameter	Value
Plasma current, I_p	400 kA
Plasma density, n_e	$4 \times 10^{19}\ \mathrm{m^{-3}}$
Camera pulse	29840
RCP pulse	29023

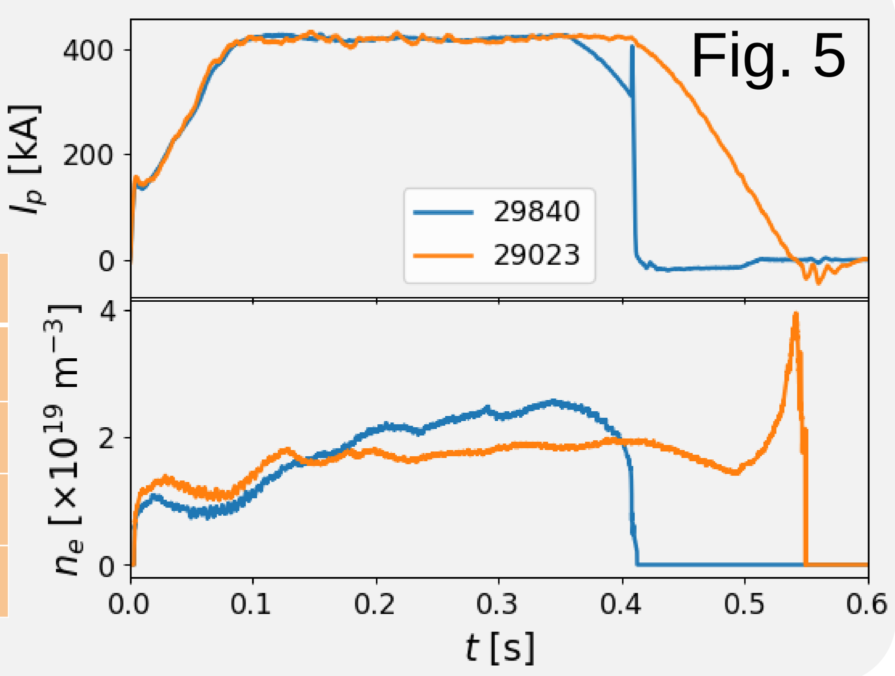

Fig. 5

SOL profiles

- **Fig. 6** shows intensity **time series** $I(t)$ for the two diagnostics at the separatrix, $r_{sep} = 0\ cm$
  - **Both** show similar intermittent bursts
  - **Camera** has flatter background due to background subtraction and non-negative SART inversion
  - Peaks with $I > I_{thresh} = \mu + 2.5\,\sigma$ labelled
- **Fig. 7** shows the **conditional average** waveforms for each diagnostic for peaks above I_{thresh}
  - **Both** highly **symmetrical** as previously seen in MAST [4]
    - Absence of sharp rising edge and long tail
  - Broader **camera** waveform τ_{rise}/τ_{fall}: $24/26\ \mu s$ vs $5/7\ \mu s$
- **Fig. 8** compares the **radial profiles** of the statistical moments of I
  - **Mean** profile shows typical exponential fall off with slight flattening in far SOL
  - **Skewness** increases radially before dropping in PFC shadow
  - Good general agreement between diagnostics up to PFC shadow

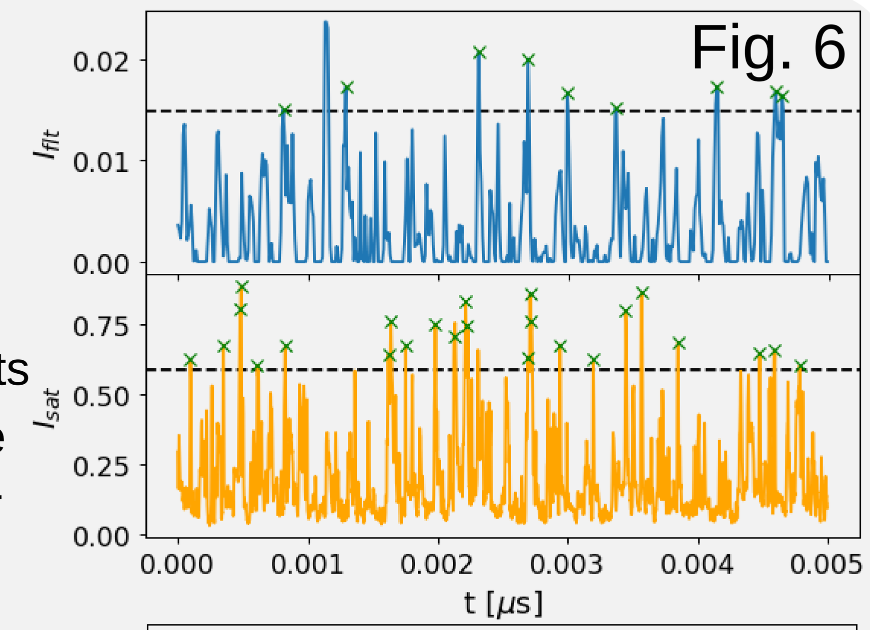

Fig. 6

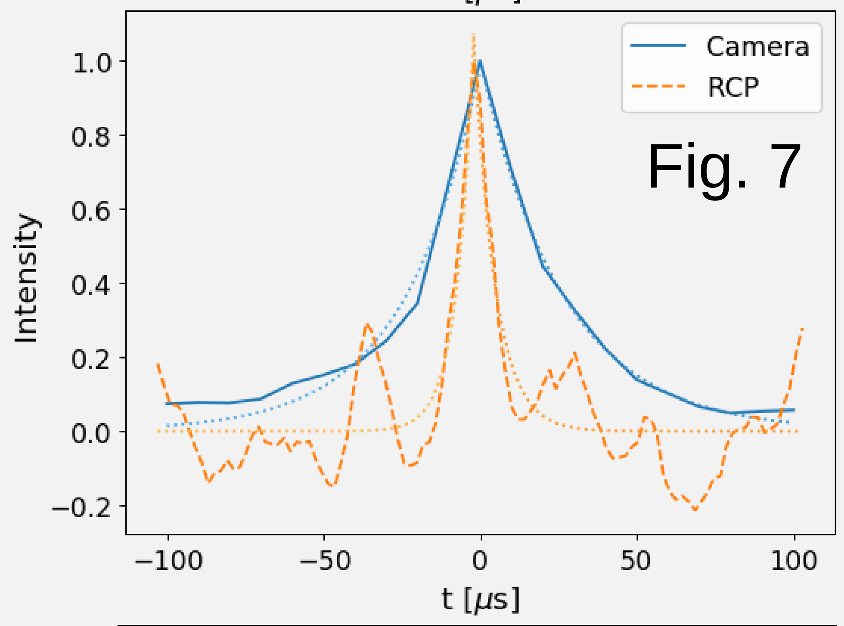

Fig. 7

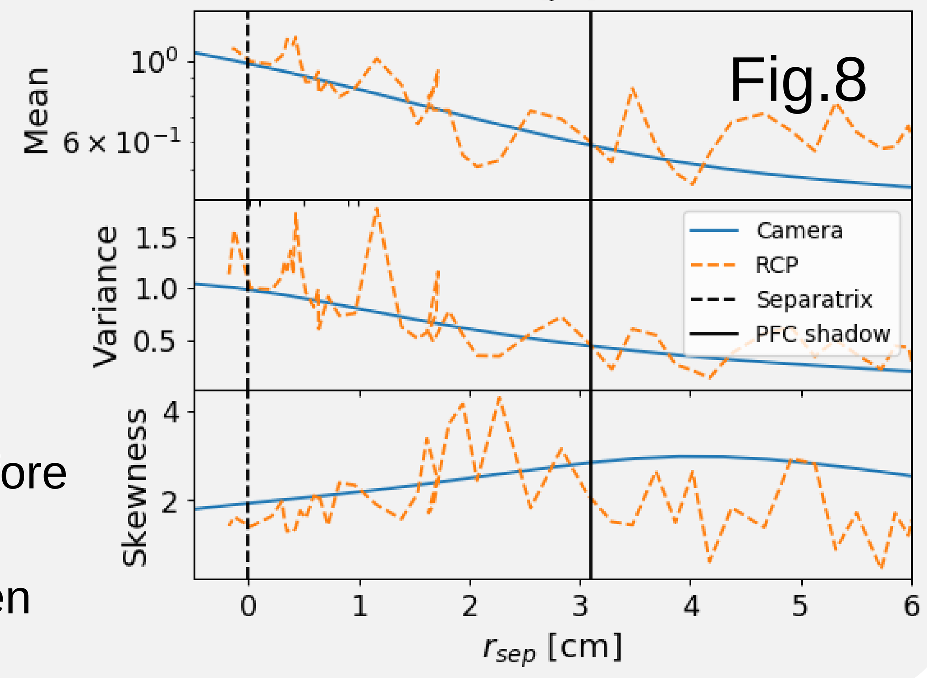

Fig.8

Filament statistics

- **Fig. 9** is the distribution of **waiting times** τ_{wait} from each diagnostic
  - Exponential distribution indicative of **Poisson process**
  - For same I_{thresh} **camera** has longer τ_{wait}: $560\ \mu s$ vs $110\ \mu s$
  - **Camera** requires $I_{thresh} = \mu + 0.2\,\sigma$ for same τ_{wait} as **RCP**
- **Fig. 10** shows the **autocorrelation function** for the two techniques
  - Fit: $A_{fit}(t) = \exp\left[-(t/\tau_{ac})^{\beta-1}\right]$,
  - As seen with conditional average the **camera** gives longer auto-correlation times, τ_{ac}: $40\ \mu s$ vs $9\ \mu s$
- **Fig. 11** gives dependence of **flatness**, $F(I)$, of I as a function of the **skewness**, $S(I)$
  - Well described by $F = {}^3/_2\, S^2$ indicating I fluctuation PDF follows a Gamma distribution
- Measurements of filament statistics are useful to feed into analytic framework [2] for modelling of SOL profiles from filament properties

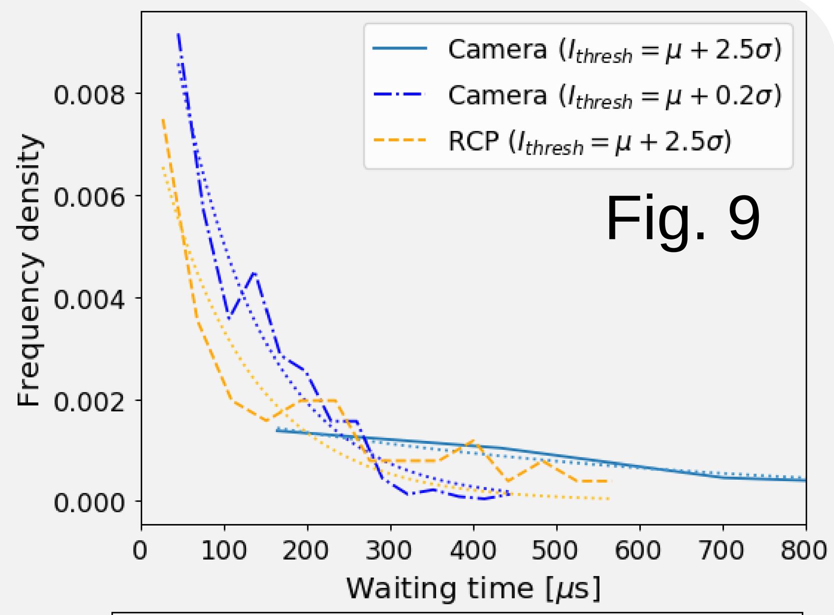

Fig. 9

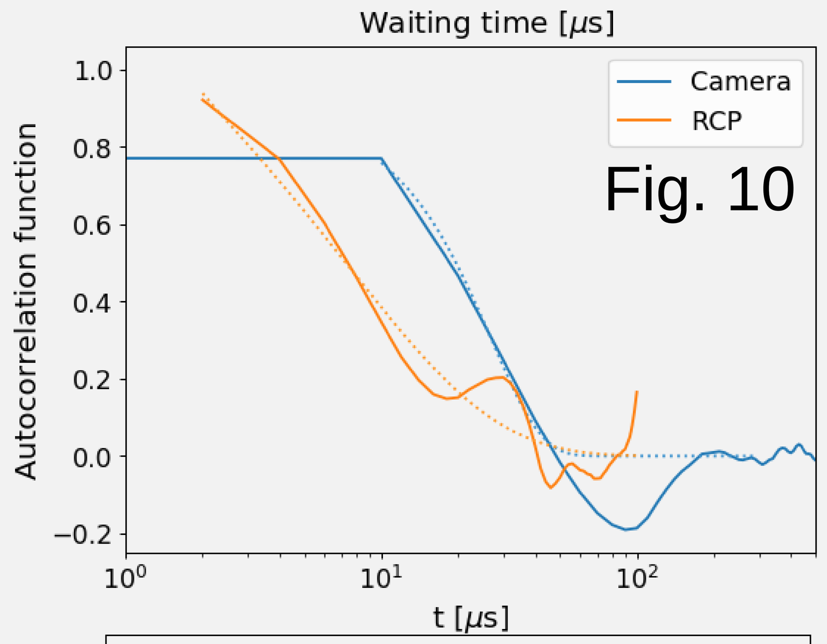

Fig. 10

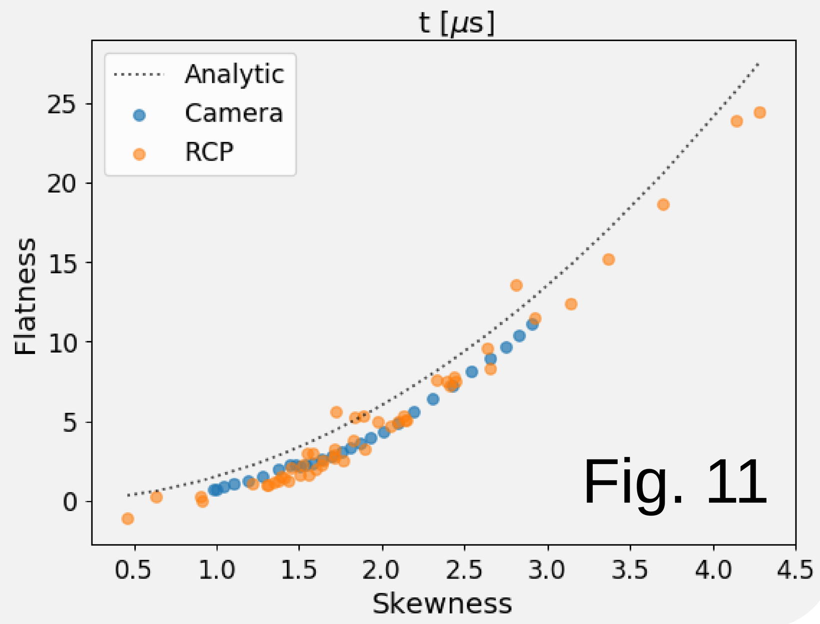

Fig. 11

Conclusions

- **RCP** filament analysis techniques successfully applied to visible **camera** data
- **Radial profiles** of mean, variance and skewness of intensity agree well
- **Conditionally averaged peaks** share symmetrical double exponential shape
- **Flatness vs skewness** indicates I fluctuations follow a Gamma distribution
- **Peak widths**, $\tau_{\mathrm{rise/fall}}$, higher for **camera** likely due to "field line shadowing"
- **Waiting times**, τ_{wait}, ~×5 longer for **camera** likely due to increased widths

This work was funded by the RCUK Energy Programme [grant EP/P012450/1] and the Engineering and Physical Sciences Research Council [grant EP/K504178/1]

For further information on data and models please contact publicationsmanager@ccfe.ac.uk.

References
[1] D'Ippolito *et al.*, PoP, 18(6), 60501 (2011)
[2] Militello, F. & Omotani, J. T., NF, 56(10), 104004 (2016)
[3] Militello, F., & Omotani, J. T. PPCF, 58(12), 125004. (2016)
[4] Militello *et al.*, PPCF, 55(2), 25005 (2013)